

Numerical Study of Separated Flows in Backward Facing Step by Using Collocated Grid Arrangement

Dr. Ahmed Waheed Mustafa, Lecturer
Mechanical Engineering Department- University of Tikrit

Abstract

The effects of Reynolds number and the inlet height ratio on separated flow over backward facing step are investigated. The flow field is studied numerically with different inlet height ratio. The laminar flow field is analyzed numerically by solving the steady, two-dimensional incompressible Navier-Stokes equations. A collocated (non-staggered) grid is used in the momentum equations, which discretized by finite volume method, SIMPLE algorithm is used to adjust the velocity field to satisfy the conservation of mass. The range of Reynolds number is ($Re = 100 - 800$). The results show that at low height ratio ($h/H = 0.25$) and high Reynolds number the flow separated along the top wall of the channel. Good agreement with the experimental data is obtained.

Keywords: Backward Facing, Separation, Finite Volume, Collocated Grid

دراسة عددية للجريان المنفصل في درجة خلفية باستخدام ترتيب الشبكة المتحددة الموقع

الخلاصة

تم دراسة تأثير رقم رينولد و نسبة ارتفاع الدخول على الجريان المنفصل في درجة خلفية. تمت دراسة حقل الجريان عدديا لنسب ارتفاع دخول مختلفة. حقل الجريان الطباقى تم تحليلية عدديا بحل معادلات نافير ستوك للجريان المستقر والثنائي البعد. تم استخدام شبكة متحدة الموقع لتقطيع معادلات الزخم باستخدام طريقة الحجم المحدد. خوارزمية (SIMPLE) استخدمت لتصحيح حقل السرعة لتحقيق حفظ الكتلة. مدى رقم رينولد هو (100-800). بينت النتائج انه عند نسبة ارتفاع عند الدخول قليلة ($h/H=0.25$) ورقم رينولد عالي فإن الجريان ينفصل على السطح العلوي للقناة. توافق جيد بين نتائج البحث والنتائج العملية تم الحصول عليه.

الكلمات الدالة: درجة خلفية، فصل، حجم محدود، جسيمات مجمعة

Nomenclatures

F mass flux
H Total channel height
h Inlet channel height
L Length of the channel
P Dimensionless Pressure
Re Reynolds number
U Dimensionless axial velocity
V Dimensionless vertical velocity
 X_r Dimensionless Reattachment length
X Dimensionless axial coordinate

Y Dimensionless vertical coordinate

Subscripts

e East face of the control volume
n North face of the control volume
s South face of the control volume
w West face of the control volume

Superscripts

* Old value
' Corrected Value

Introduction

The separated flow generated as fluid passes over a backward-facing step is of interest for a variety of reasons. First, separated flows produced by an abrupt change in geometry are of great importance in many engineering applications. Also, the backward-facing step is an extreme example of separated flows that occur in aerodynamic devices such as high-lift airfoils at large angles of attack. In these flows separation may be created by a strong adverse pressure gradient rather than a geometric perturbation, but the flow topology is similar. Secondly, from a fundamental perspective, there is a strong interest in understanding instability and transition to turbulence in plane channels and pipes.

The flow over a backward facing step (BFS) was studied extensively to understand the physics of such separated flows. The BFS has the most features of separated flows, such as separation, reattachment, recirculation, and development of shear layers. Armaly et al. [1] studied laminar, transition, and turbulent isothermal flow over a BFS experimentally. Also, numerical studies in the laminar regime for isothermal flow were conducted by Armaly et al. [1] and by Durst and Periera [2]. Additional numerical work for a two-dimensional isothermal flow over a BFS was conducted by Gartling [3], Kim and Moin [4], and Sohn [5].

All numerical methods were presented in the previous studies used a staggered grid.

In the present study the non staggered grid Peric et al. [6] is used to predict the reattachment length of the separated flow and the effect on the height ratio.

Governing Equations

The basic flow configuration, under study, is shown in figure 1. The flow is considered to be two-dimensional,

laminar, steady, constant fluid properties, and incompressible. The dimensionless continuity, and momentum, equations in Cartesian coordinates are given as

$$\frac{\partial U}{\partial X} + \frac{\partial V}{\partial Y} = 0 \quad \dots\dots\dots(1)$$

$$\frac{\partial(U^2)}{\partial X} + \frac{\partial(UV)}{\partial Y} = -\frac{\partial P}{\partial X} + \frac{1}{Re} \left(\frac{\partial^2 U}{\partial X^2} + \frac{\partial^2 U}{\partial Y^2} \right) \quad (2)$$

$$\frac{\partial(UV)}{\partial X} + \frac{\partial(V^2)}{\partial Y} = -\frac{\partial P}{\partial Y} + \frac{1}{Re} \left(\frac{\partial^2 V}{\partial X^2} + \frac{\partial^2 V}{\partial Y^2} \right) \quad (3)$$

Where

$$X=x/H, Y=y/H, U=u/U_{bulk}, V=v/U_{bulk}, P=p/\rho U_{bulk}^2, Re = U_{bulk} H/\nu.$$

Configuration and Boundary Conditions

The basic flow configuration, under study, is shown in figure 1. The boundary conditions used in the numerical solution are also illustrated in figure 1. A parabolic inlet velocity profile is assumed which is given by:

$$U_{in}=u/U_{bulk}=\delta Y_b(1-Y_b) \quad (4)$$

Where $Y_b=(y-(H-h))/h$

Discretization of the Flow Equations

The governing equations are discretized by using the finite volume method based on non-staggered (collocated) grid. Since all variables are stored in the center of the control volume, the interpolation method is used to avoid the decoupling between velocity and pressure; this interpolation method is presented in this paper.

The continuity and the momentum equations are discretized over the collocated grid shown in figure 2.

By integrating the x-momentum equation (3) over the control volume shown in figure (2), we have

$$[UU\Delta Y]_w^e + [UV\Delta X]_s^n = -(P_e - P_w)\Delta Y|_P + \frac{1}{\text{Re}} \left[\frac{\partial U}{\partial X} \Delta Y \right]_w^e + \frac{1}{\text{Re}} \left[\frac{\partial U}{\partial Y} \Delta X \right]_s^n \quad (5)$$

For numerical stability, the convection term (left side of equation (5)) are approximated by the upwind differencing scheme (UDS), Patankar [7] as

$$[UU\Delta Y]_w^e = U_e F_e - U_w F_w = [U_P \max(F_e, 0) - U_E \max(-F_e, 0)] - [U_W \max(F_w, 0) - U_P \max(-F_w, 0)] \quad (6)$$

Where $F_e = (U\Delta Y)_e$, $F_w = (U\Delta Y)_w$, are the mass flux at the control volume faces e and w respectively.

By the same scheme the second convective term can be approximated as

$$[UV\Delta Y]_s^n = U_n F_n - U_s F_s = [U_P \max(F_n, 0) - U_N \max(-F_n, 0)] - [U_S \max(F_s, 0) - U_P \max(-F_s, 0)] \quad (7)$$

Where $F_n = (V\Delta X)_n$, $F_s = (V\Delta X)_s$, are the mass flux at the control volume faces n and s respectively.

The diffusion terms can be approximated by the center difference scheme (CDS) as

$$\frac{1}{\text{Re}} \left[\frac{\partial U}{\partial X} \Delta Y \right]_w^e = D_e(U_E - U_P) - D_w(U_P - U_W) \quad (8)$$

$$\text{Where } D_e = \left(\frac{\Delta Y}{\text{Re} \Delta X} \right)_e, D_w = \left(\frac{\Delta Y}{\text{Re} \Delta X} \right)_w$$

$$\frac{1}{\text{Re}} \left[\frac{\partial U}{\partial Y} \Delta X \right]_s^n = D_n(U_N - U_P) - D_s(U_P - U_S) \quad (9)$$

$$\text{Where } D_n = \left(\frac{\Delta X}{\text{Re} \Delta Y} \right)_n, D_s = \left(\frac{\Delta X}{\text{Re} \Delta Y} \right)_s$$

Substituting of eqs. (6), (7), (8), and (9) into equ.(5) gives:-

$$a_P U_P = \sum_{nb} a_{nb} U_{nb} + (1 - \alpha_U) a_P U_P^0 - (P_e - P_w)\Delta Y|_P \quad (10)$$

Where the index (nb) runs over all neighbouring points E , W , N , and S , and

$$a_E = D_e + \max(-F_e, 0) \quad (11a)$$

$$a_W = D_w + \max(F_w, 0) \quad (11b)$$

$$a_N = D_n + \max(-F_n, 0) \quad (11c)$$

$$a_S = D_s + \max(F_s, 0) \quad (11d)$$

$$a_P = \sum_{nb} a_{nb} / \alpha_U \quad (11e)$$

Where (α_U) is the under-relaxation parameter, necessary for stability Patankar [7]. The quantity U_P^0 in equation (10) indicates the value of U_P from the previous iteration. For the collocated arrangement, the coefficient in eqs. (11a-e) are same for V -equation.

Pressure-Velocity Coupling

The U - and V - momentum equations are solved using guessed values for the pressure field and mass fluxes. The velocity components U^* and V^* , calculated with these guessed values will not satisfy the continuity equation, so that the velocity components must be corrected as

$$U = U' + U^* \quad (12a)$$

$$V = V' + V^* \quad (12b)$$

Where U' , and V' are corrected velocities and can be calculated as follows:-

Rewrite the U -equation (equ. 10) for node (P) and (E) (see figure 2) as:

$$U_P^* = \left(\frac{\sum_{nb} a_{nb} U_{nb}^* + (1 - \alpha_U) a_P U_P^0 - (P_e^* - P_w^*) \Delta Y}{a_P} \right)_P \quad (13)$$

$$U_E^* = \left(\frac{\sum_{nb} a_{nb} U_{nb}^* + (1 - \alpha_U) a_P U_P^0 - (P_e^* - P_w^*) \Delta Y}{a_P} \right)_E \quad (14)$$

To find u_e^* at east face of the control volume (figure 2), we use linear interpolation except the pressure term which is calculated as in the staggered approach Rhie and Chow [8].

$$\therefore u_e^* = \overline{u_e^*} - \left(\frac{1}{a_P} \right)_e (\Delta Y)_e (P_E^* - P_P^*) \quad (15)$$

Where

$$\overline{u_e^*} = \left(\frac{\sum_{nb} a_{nb} U_{nb}^* + (1 - \alpha_U) a_P U_P^0}{a_P} \right)_e \quad (16)$$

By the same method we can find the velocities at (w , n , and s) faces as

$$u_w^* = \overline{u_w^*} - \left(\frac{1}{a_P} \right)_w (\Delta Y)_w (P_P^* - P_W^*) \quad (17)$$

$$v_n^* = \overline{v_n^*} - \left(\frac{1}{a_P} \right)_n (\Delta X)_n (P_N^* - P_P^*) \quad (18)$$

$$u_s^* = \overline{v_s^*} - \left(\frac{1}{a_P} \right)_s (\Delta X)_s (P_P^* - P_S^*) \quad (19)$$

To enforce mass conservation, velocity and pressure correction are introduced by Rhie and Chow [8]

$$u_e' = - \left(\frac{1}{a_P} \right)_e (\Delta Y)_e (P_E' - P_P') \quad (20)$$

$$u_w' = - \left(\frac{1}{a_P} \right)_w (\Delta Y)_w (P_P' - P_W') \quad (21)$$

$$v_n' = - \left(\frac{1}{a_P} \right)_n (\Delta X)_n (P_N' - P_P') \quad (22)$$

$$v_s' = - \left(\frac{1}{a_P} \right)_s (\Delta X)_s (P_P' - P_S') \quad (23)$$

The discretization of continuity equation is

$$(u \Delta Y)_e - (u \Delta Y)_w + (v \Delta X)_n - (v \Delta X)_s = 0 \quad (24)$$

To correct the velocities at the faces of the control volume:

$$u_e = u_e^* + u_e' \quad (25a)$$

$$u_w = u_w^* + u_w' \quad (25b)$$

$$v_n = v_n^* + v_n' \quad (25c)$$

$$v_s = v_s^* + v_s' \quad (25d)$$

Substituting eqs.(25) into equ.(24) yields

$$\begin{aligned} & (u'\Delta Y)_e - (u'\Delta Y)_w + (v'\Delta X)_n \\ & - (v'\Delta X)_s = S_p \end{aligned} \quad (26)$$

Where S_p is the mass source and is given by

$$\begin{aligned} S_p = & (u^*\Delta Y)_w - (u^*\Delta Y)_e + (v^*\Delta X)_s \\ & - (v^*\Delta X)_n \end{aligned} \quad (27)$$

Substituting eqs. (20, 21, 22, and 23) into equ. (26) gives:-

$$\begin{aligned} a_{PP}P'_p = & a_{EE}P'_E + a_{WW}P'_W + a_{NN}P'_N + a_{SS}P'_S + \\ & S_p \end{aligned} \quad \dots\dots (28)$$

Where

$$a_{EE} = \overline{\left(\frac{1}{a_p}\right)_e} (\Delta Y|_e)^2 \quad (29a)$$

$$a_{WW} = \overline{\left(\frac{1}{a_p}\right)_w} (\Delta Y|_w)^2 \quad (29b)$$

$$a_{NN} = \overline{\left(\frac{1}{a_p}\right)_n} (\Delta X|_n)^2 \quad (29c)$$

$$a_{SS} = \overline{\left(\frac{1}{a_p}\right)_s} (\Delta X|_s)^2 \quad (29d)$$

$$a_{PP} = a_{EE} + a_{WW} + a_{NN} + a_{SS} \quad (29e)$$

Solution Procedure

For the steady and non-staggered (collocated), the overall **SIMPLE** solution procedure takes the following steps

- (1) Assume the initial pressure field ($P^* = 0$).

- (2) Calculate the coefficient of the momentum equations from equations (11).

- (3) Solve the (U^*, V^*) momentum equation by line-by-line method of equation (10) using the guessed pressure field (P^*).

- (4) Compute the face mass flow rates (F_e^*, F_w^*, F_n^* and F_s^*) by using interpolated face velocities from equations (16, 17, 18, and 19).

- (5) Calculate the source term of the pressure correction equation from equation (27).

- (6) Calculate the coefficients of the pressure correction equation from equations (29).

- (7) Solve the pressure correction equation (28) by line-by-line method to obtain the corrected pressure field (P').

- (8) Calculate the correction of the velocities from equations (20, 21, 22, and 23).

- (9) Calculate the correction of face mass flow rates (F_e', F_w', F_n' and F_s') based on the corrected velocities calculated in step (8).

- (10) Correct the velocities by using equations (12); and face mass flow rates by

$$F_e = F_e^* + F_e' \quad (30a)$$

$$F_w = F_w^* + F_w' \quad (30b)$$

$$F_n = F_n^* + F_n' \quad (30c)$$

$$F_s = F_s^* + F_s' \quad (30d)$$

Correct the control volumes pressure by underrelaxed the pressure correction as

$$(P = P^* + \alpha_p P') \quad \dots\dots\dots (31)$$

Return to step 1 and repeat step 1 to 11 until the convergence is attained.

For each variable, the sum of the absolute value of the residuals over all the control volume is calculated, and normalized by an appropriate quantity F_n , typically the inlet mass or momentum flux, this normalized sum of the absolute residuals should be satisfies

$$\frac{\sum R^k}{F_n} \leq \lambda \quad (32)$$

Values of λ used in calculations were of order 10^{-3} .

Grid Independence

The table below shows the results of the reattachment length (X_r) obtained for the grid independence study for the case $Re = 400$, and $h/H = 0.5$. A grid size of 61X21 (61 in X direction and 21 in Y direction) gives a grid independence solution.

Grid Size(MXN)	Reattachment Length
31X21	3.98
41X21	4.05
51X21	4.22
61X21	4.3
61X31	4.3

Validation

The numerical solution is validated by comparing results of the reattachment length (X_r) with the experiment of Armaly et al. [1] and with the

numerical results of staggered grid of Eiyad Abu-Nada ^[9] for different Reynolds number (Re) for the case ($h/H = 0.5$). Figure 3 shows good agreement between the present results and the experiment of Armaly et al. [1].

Results

Three inlet height ratio ($h/H = 0.25, 0.5, 0.75$) are considered. The channel length (L) is set to 10 H.

In figure 4 the contours of the predicted streamlines are shown for Reynolds number (100-800) and for ($h/H = 0.25$). Two recirculation flow zones are encountered for $Re > 400$ the primary recirculation zone occurs directly downstream the step at the bottom wall of the channel, whereas the other secondary recirculation zone exists along the top wall. However, for lower Reynolds numbers, such as $Re < 400$, only the bottom recirculation zone appears. In this geometry the flow is descend from small area to sudden enlargement so that the velocity decreased and adverse pressure gradient created, this adverse pressure causes the separation along the top wall as shown in figure (4c-e).

In figure 5 the contours of the predicted streamlines are shown for Reynolds number (100-800) and for ($h/H = 0.5$). As Reynolds number decreases the secondary recirculation zone that exists along the top wall begins to disappear. However, for lower Reynolds numbers, such as $Re = 400$, only the bottom recirculation zone appears.

In figure 6 the contours of the predicted streamlines are shown for Reynolds number (100-800) and for ($h/H = 0.75$). In this configuration the secondary recirculation zone exists along the top wall is totally disappears, and the flow just separated downstream the step at the bottom wall of the channel.

Conclusions

The finite volume method with collocated grid is used to analyze the flow field over backward facing step for two dimensional steady flows. The results show that at low height ratio ($h/H = 0.25$) and high Reynolds number, in addition to the separation that occur down the step the flow also separated along the top wall of the channel.

References

- 1-Armaly B.F., Durst F., Pereira J.C.F, and Schönung, Experimental and Theoretical Investigation of Backward-Facing Step fFow, *J. Fluid Mechanics* 1983; 127: 473-496.
- 2- Durst F. and Pereira J.C.F, Time-dependent laminar backward-facing step flow in a two-dimensional duct, *J. Fluid Engineering* 1988; 110: 289-296.
- 3-Gartling D.K., A test problem for outflow boundary condition-Flow over a backward facing step, *Int. J. Num. Methods Fluids* 1990; 11: 953-967.
- 4-Kim J., and Moin P., Application of a fractional-step method to incompressible Navier-Stokes Equations, *J. Computational Physics* 1985; 59: 308-323.
- 5- Sohn J., Evaluation of FIDAP on some classical laminar and turbulent Benchmarks, *In J. Num. Methods Fluids* 1988; 8: 1469-1490.
- 6- Peric, M., Kessler, R., Scheuerer, G., Comparison of finite volume numerical methods with staggered and collocated grid. *Computers and fluid*, 1988, 16, 389- 403.
- 7-Patankar, S.V., Numerical Heat Transfer and Fluid Flow, New York, Hemisphere Publishing Corporation, Taylor and Francis Group, 1980.
- 8- Rhie, C. M., and Chow, W. L., Numerical Study of the Turbulent Flow Past an Airfoil with Trailing Edge Separation, *AIAA Journal*, 1983, Vol.21, PP 1525-1532.
- 9-Eiyad Abu-Nada, Numerical Prediction of Entropy Generation in Separated Flows, entropy, 2005, PP 234-252.

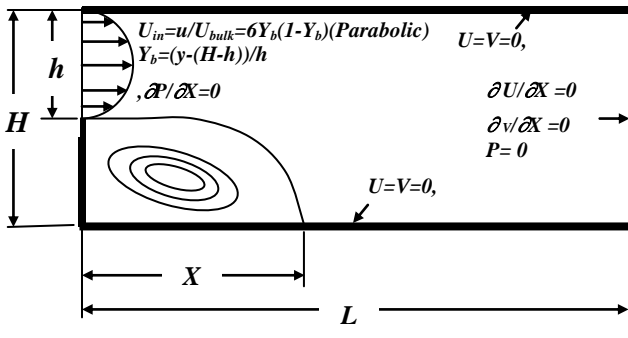


Figure (1) Geometry and Boundary Conditions

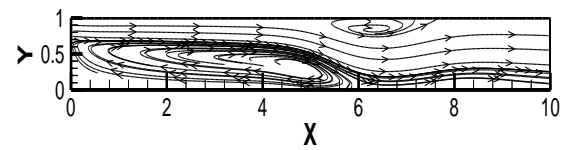
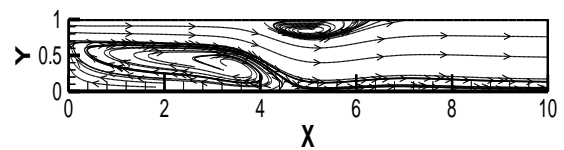
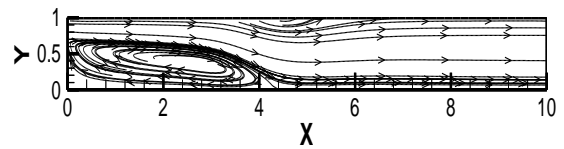
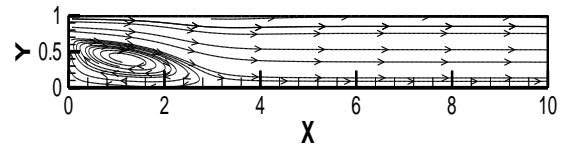
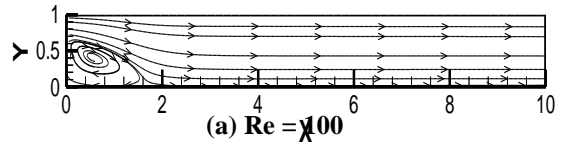


Figure (4) The effect of Reynolds number on the streamlines for flow configurations ($h/H = 0.25$).

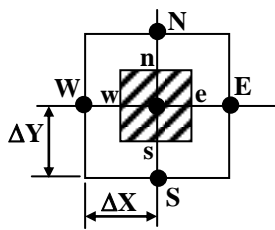


Figure (2) Control Volume

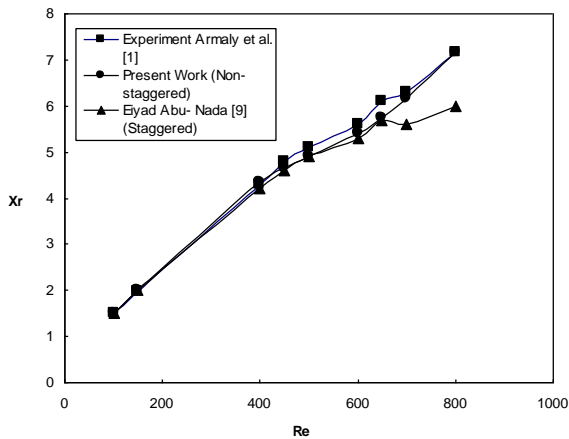


Figure (3) Comparison of the reattachment length with the Reynolds number for present and previous works for the case $h/H=0.5$.

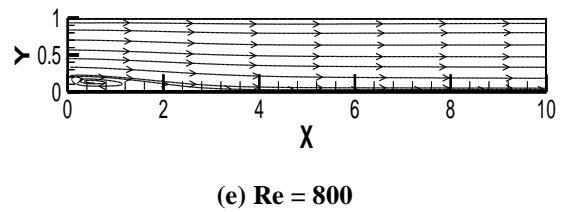
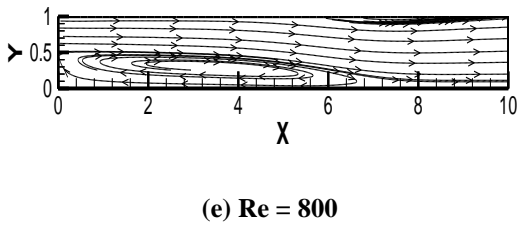
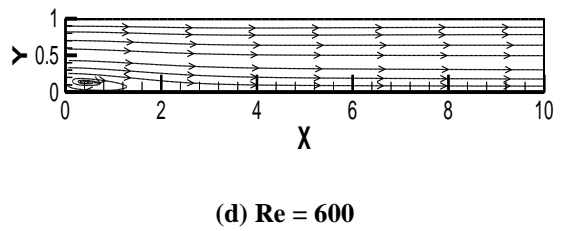
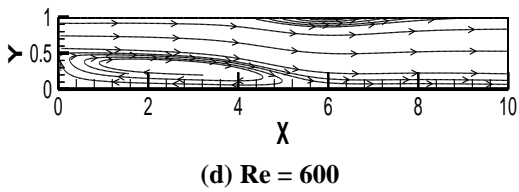
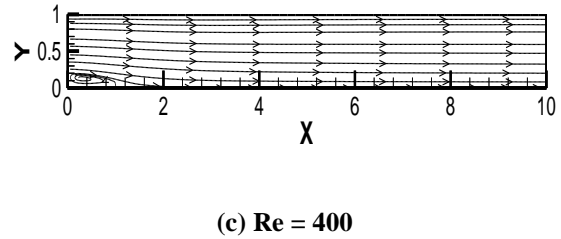
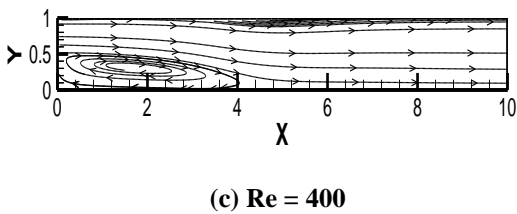
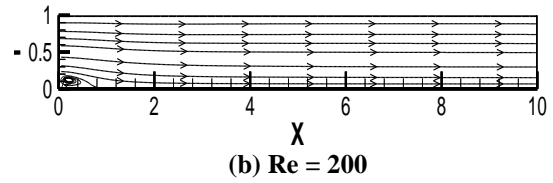
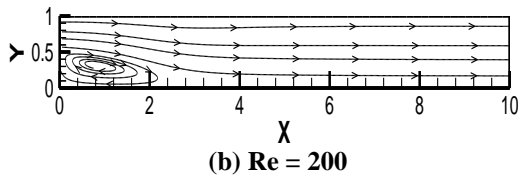
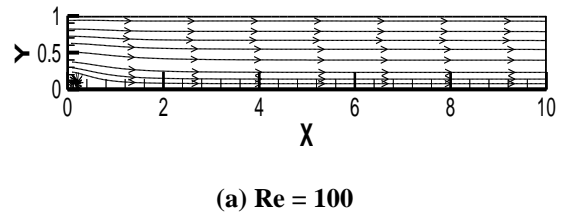
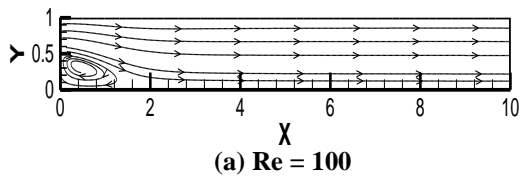


Figure (5) The effect of Reynolds number on the streamlines for flow configurations ($h/H = 0.5$).

Figure (6) The effect of Reynolds number on the streamlines for flow configurations ($h/H = 0.75$).